Enhanced Goos–Hänchen shift of the reflected and transmitted defect modes from a one-dimensional photonic crystal containing an all-dielectric elliptical metamaterial defect layer

Amir Madani[1*], Simin Shirin[1], Nasrin Shahbazi[1], Davod Jafari[1]

[1]*Department of Laser and Optical Engineering, University of Bonab, Bonab, Iran*

Received: 2026-06-20 Final revised: 2026-07-01 Accepted: 2026-09-10

Abstract

The Goos–Hänchen lateral shifts of the TM-polarized defect modes, both in reflection and transmission, have been theoretically investigated for a 1D photonic crystal featuring an all-dielectric elliptical metamaterial defect layer, with the analysis conducted in the near-infrared range. The reflection and transmission spectra of the structure exhibited a wide photonic band gap in this region of wavelength, with defect modes dependent on the angle of incidence. The results showed that the wavelengths of the defect modes shifted toward shorter wavelengths with an increase in the incidence angle. Besides, the reflectance and the transmittance of the defect modes varied noticeably with changes in the incidence angle. It was revealed that the relative Goos–Hänchen shifts of the reflected modes have negative values, while the relative shifts of the transmitted modes are positive. Also, the increasing behavior of the lateral shifts at the defect mode conditions has been exhibited by the results. The maximum value of $\Delta_r = -9.5\lambda$ at $\lambda_d = 1409.9$ nm and $\theta = 60^\circ$, and $\Delta_t = +89.7\lambda$ at $\lambda_d = 1482.5$ nm and $\theta = 40^\circ$ have been obtained for the reflected and transmitted modes, respectively. Finally, the electric field profiles of the incident, reflected, and transmitted Gaussian beams for the case of $\lambda_d = 1409.9$ nm and $\theta = 60^\circ$ verified the increased lateral shift of the beams at the interface of the photonic crystal.

Keywords: All-dielectric elliptical metamaterial, Goos–Hänchen shift, Defect mode.

[*] **Email:** a-madani@ubonab.ac.ir

1. Introduction

It is now well recognized that the reflection of light beams at the boundary between two different media can deviate from the classical predictions of Snell's law, and the reflected beam experiences a lateral shift relative to the geometric-optics expectation. This lateral movement, defined as the Goos–Hänchen shift (GH), arises from the different phase changes acquired by the various plane wave constituents of the beam upon reflection. This phenomenon was first discovered experimentally by Goos and Hänchen in 1947 [1] and later formulated theoretically by Artmann[2]. Initial studies on the GH displacement focused on total internal reflection, but subsequent works have extended the issue to partial reflection and transmission[3-5].

The GH shift has recently become a topic of significant research attention, owing to its potential for real-world implementation in areas like optical sensors[6-9], optical switches[10], chemical sensors[11], polarizers[12], lasers[13], filters[14], and integrated optics[15, 16]. This growing interest has motivated extensive studies of the phenomenon in a broad range of optical architectures, including multilayer structures[17-19], photonic crystals[20-22], left-handed materials[23-25], antiferromagnetic materials[26, 27], metamaterials[28, 29], nonabsorbing and absorbing platforms[30-32], graphene-based media[33, 34], and structurally chiral media[35-37].

The Goos–Hänchen lateral displacement may assume either positive or negative values; however, its amplitude is generally extremely small, typically on the order of a small fraction of the optical wavelength, and difficult to observe experimentally. Therefore, various methods have been examined to enhance the GH shift, such as beam-shaping techniques [38-41], transformation optics [42], and the excitation of surface waves [43-46]. Moreover, the introduction of defect layers within layered structures has emerged as another efficient approach for achieving enhanced shifts. For instance, remarkable lateral shifts near defect modes in a one-dimensional photonic crystal (1DPC) have been demonstrated by Wang et al. [47], while Chen et al. described the same effects in nonlinear photonic crystals [48]. Zhao et al. investigated large GH shifts in defective photonic crystals containing graphene monolayers [49]. Yang et al studied the enhanced GH shift in a defective Pell quasiperiodic photonic crystal with monolayer MoS_2 [50]. Also, the GH shift has been investigated in a 1DPC containing a single Weyl semimetal layer as a defect [51].

All-dielectric elliptical metamaterials (EMMs) are a kind of anisotropic metamaterial representing elliptical iso-frequency contours for TM-polarized waves, which is different from conventional isotropic dielectrics. Also, in contrast to hyperbolic metamaterials, EMMs are capable of manipulating light without absorption losses. So, in the recent years, EMMs have gained more interest among researchers due to their practical capability in the design of various optical devices. For example, broad-angle negative refraction in an EMM slab was reported by Sayem et al. [52]. She et al. reported the use of EMMs in the design of high-performance polarizers [53]. Nanoscale light confinement using an elliptical metamaterial has been reported by Jahani et al. [54]. Wu et al. studied the existence of Tamm plasmon polaritons (TPPs) with high angular tunability at the interface between a metal layer and a 1DPC comprising EMMs [55]. Besides, photonic band-gap (PBG) engineering in 1DPCs comprising elliptical metamaterials has been extensively investigated by Wu et al. [56, 57].

In the present paper, we will investigate the GH lateral displacement in a 1DPC containing a layer of EMM as a defect layer, for the TM-polarized waves. TE-polarized

waves is excluded from the study because the EMM defect layer represents a conventional circular dispersion for TM polarization, which is the same as isotropic dielectrics. The transfer matrix method has been employed to obtain the reflection and transmission spectra of the structure. The results show the existence of the defect modes inside the photonic band gap of the 1DPC. Besides, the phases of the reflection and transmission coefficients of the structure have been obtained, which show a noticeable phase change around the defect mode position. Also, we have calculated the GH displacement of the TM-polarized reflected and transmitted Gaussian beams and showed that the magnitude of the shifts increased remarkably for the cases of the defect modes. The influence of the incidence angle on both the wavelength position of defect modes and their associated GH lateral shifts has been investigated. To validate the obtained findings, field profile plots of the reflected and transmitted beams have been provided.

2 .Theory and Methodology

Fig. 1 illustrates our proposed structure denoted as $(AB)^5V(AB)^5$, which is a defective 1DPC embedded in air. The constituent layers of the photonic structure are specified as follows: layer A is silicon (Si) with a relative permittivity $\varepsilon_A = 3.48^2$, and layer B is silicon dioxide (SiO_2) with $\varepsilon_B = 1.44^2$ [58]. The thicknesses are $d_A = 120$ nm and $d_B = 240$ nm. The central defect layer, denoted V, is designed as an effective medium material formed in the sequence $(CD)^5$, where C is Si and D is SiO_2. Since the thickness of each C and D sublayer is significantly smaller than the near-infrared wavelengths under investigation, the effective medium theory has been adopted to describe the electromagnetic behavior of the EMM layer.

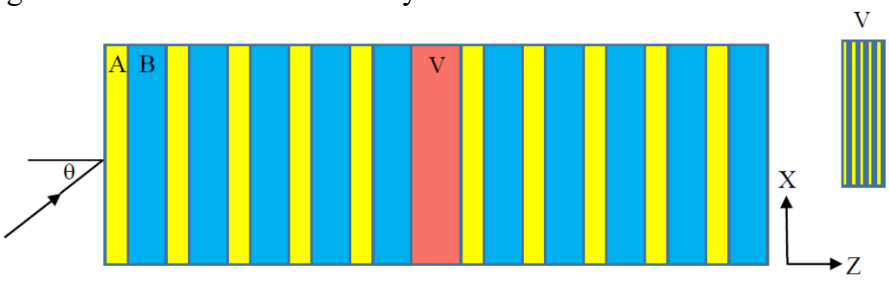


Fig. 1. Schematic diagram of the proposed defective structure composed of Si layers (A) and SiO_2 layers (B). The defect layer V is EMM and is assumed to be formed by combining thin, subwavelength Si and SiO_2 layers.

Under this approximation, the EMM can be treated as an effective uniaxial material whose optic axis is directed along the z-axis, i.e., normal to the plane of the layers. The relative permittivity tensor of the EMM layer is given by $\overline{\varepsilon_V} = [\varepsilon_{Vx}, \varepsilon_{Vy}, \varepsilon_{Vz}]$ [56, 57], where

$$\varepsilon_{Vx} = \varepsilon_{Vy} = f\varepsilon_C + (1-f)\varepsilon_D \quad and \quad \varepsilon_{Vz} = \frac{\varepsilon_C \varepsilon_D}{f\varepsilon_D + (1-f)\varepsilon_C}. \tag{1}$$

Here, $f = 0.8$ is the filling factor, representing the filling ratio of the C layers, where the thickness of the defect layer is $d_V = 125$ nm.

Starting from Maxwell's equations and employing the relative permittivity tensor $\overline{\varepsilon_V}$ for the EMM layer, a straightforward algebraic procedure leads to the TM polarization dispersion relation, given by:

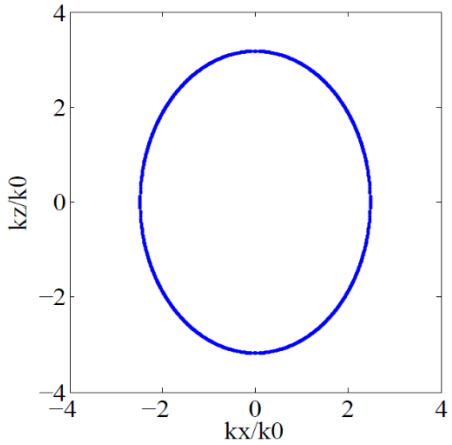


Fig. 2. Iso-frequency curve diagram of the proposed defect layer (EMM layer) for TM polarization.

$$\frac{k_x^2}{\varepsilon_{Vz}} + \frac{k_{zV}^2}{\varepsilon_{Vx}} = k_0^2, \tag{2}$$

where k_0 is the vacuum wavevector of the incident waves, $k_x = k_0 \sin\theta$ is the tangential component of the wavevector, k_{zV} is the normal component of the wavevector inside the EMM layer, and θ is the incident angle. The dispersion (iso-frequency) curve of the EMM layer, derived from Eq.2, is illustrated in Fig. 2. This figure clearly verifies the elliptical dispersion relation characteristic of the TM-polarized waves propagating in the effective medium.

Using the stationary-phase technique, the GH lateral shifts of the reflected and transmitted beams in the proposed 1DPC can be obtained, with the displacement expressed as $\Delta_r = -\frac{d\varphi_r}{dk_x}$ and $\Delta_t = -\frac{d\varphi_t}{dk_x}$, where φ_r and φ_t are the phases of the reflection and transmission coefficients [59]. However, this method becomes inaccurate when φ_r and φ_t vary rapidly with k_x. Under such circumstances, an alternative approach utilizing the normalized first moment of the field intensity distribution can be adopted. This approach evaluates the average transverse position of the beam's energy distribution. For a narrow Gaussian incident beam, the reflected and transmitted field amplitudes can thus be obtained from the incident field amplitude as [60]:

$$U_r(x) = \frac{1}{2\pi}\int_{-\infty}^{+\infty} r(k_x)U_i(k_x)e^{-i\,k_x x}dk_x \tag{3}$$
$$U_t(x) = \frac{1}{2\pi}\int_{-\infty}^{+\infty} t(k_x)U_i(k_x)e^{-i\,k_x x}dk_x$$

Here, $r(k_x)$, $t(k_x)$, and $U_i(k_x)$ denote the reflection coefficient, the transmission coefficient, and the Fourier spectrum of the incident beam, respectively. The coefficients $r(k_x)$ and $t(k_x)$ are determined by applying the transfer-matrix method as detailed in Ref. [61]. The incident beam is assumed to be a narrow Gaussian beam with width a, and its field amplitude is given by

$$U_i(x) = e^{\left(-\left(\frac{x^2}{4a^2}\right)+ik_{xi}x\right)} \tag{4}$$

Subsequently, the relative lateral GH shift of the reflected and transmitted beams can be defined as

$$\Delta_r = \frac{1}{a}\frac{\int_{-\infty}^{+\infty} x|U_r(x)|^2dx}{\int_{-\infty}^{+\infty}|U_r(x)|^2dx} \quad and \quad \Delta_t = \frac{1}{a}\frac{\int_{-\infty}^{+\infty} x|U_t(x)|^2dx}{\int_{-\infty}^{+\infty}|U_t(x)|^2dx}. \tag{5}$$

3 . Results and Discussion

We begin our analysis by plotting the reflection and transmission spectra of the defective 1DPC for TM-polarized waves, as shown in Fig. 3(a) and Fig. 3(b). Here, Fig. 3(a) represents the reflection of the structure as a function of wavelength and incidence angle in the wavelength range of 1000–2500 nm. It is evident from the figure that a wide photonic band gap is present in this spectral region. The width of the PBG, as well as its lower and upper boundaries, depends on the angle of incidence. As the incidence angle increases, the PBG width decreases while both edges display a blue shift. In addition, a narrow spectral feature with diminished reflectance, indicative of defect modes, is observed within the PBG. The defect-mode wavelength likewise exhibits a blue shift with increasing incidence angle. Fig. 3(b) represents the transmission of the structure as a function of wavelength and incidence angle, which verifies the results of Fig. 3(a).

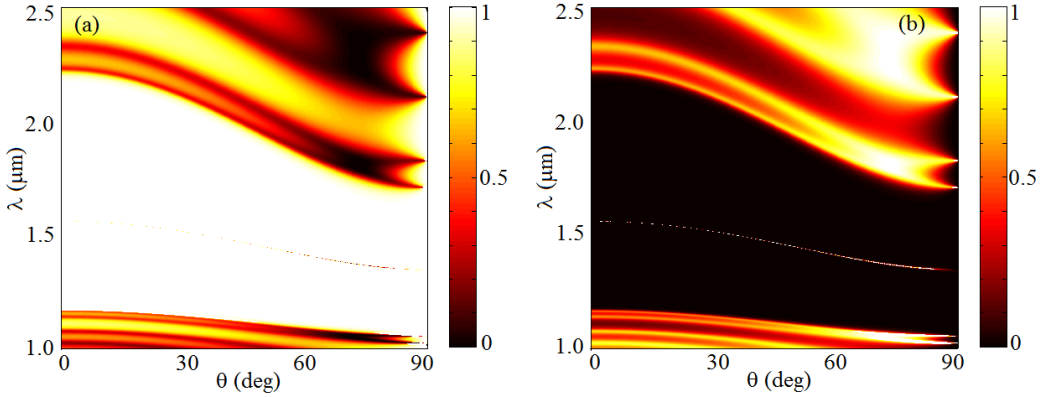


Fig. 3. (a) Reflectance and (b) transmittance of the proposed defective structure as a function of wavelength and incidence angle for TM polarization.

To obtain more information about the wavelength, reflectance, and transmittance of the defect modes, we have plotted the reflection and transmission spectra of the structure as a function of wavelength for various incidence angles in Fig. 4(a) and Fig. 4(b). It is shown that the defect mode wavelength is $\lambda_d = 1559.6$ nm for the case of normal incidence of the wave, while it shifts to $\lambda_d = 1409.9$ nm for the case of $\theta = 60^{\circ}$. Besides, it is clear from the figures that the reflectance and transmittance of the defect modes change from $R = 0.68\,, T = 0.32$ for $\theta = 0^{\circ}$ to the values of $R = 0.22\,, T = 0.78$ for $\theta = 60^{\circ}$. So, the intensity of the transmitted defect mode is higher for the larger incidence angles. The data obtained from Fig. 4(a) and Fig. 4(b) are listed in Table 1.

To investigate the increased GH shift of the reflected and transmitted defect modes, we have illustrated the phase variation of the reflection and transmission coefficients of the defective structure for the TM polarization in Fig. 5(a)-Fig. 5(f), respectively. Resonance is a specific condition that occurs when light interacts with a defect mode in a photonic crystal. The phase of the reflected and transmitted light undergoes a rapid, sharp change. Since the GH shift is essentially the spatial derivative of this phase with respect to the angle of incidence, this rapid phase change causes the reflected and transmitted beams to shift laterally by large amounts. Fig. 5(a)-Fig. 5(c) represent the phase of the reflection coefficient (φ_r) as a function of the incidence angle for different values of defect mode wavelengths (λ_d) listed in Table 1. As is clear from the figures, a pronounced positive slope appears near the incidence angles associated with the corresponding defect modes. So, large values of negative GH shift are predicted for the

TM-polarized reflected defect modes regarding the relation of GH lateral shift, $\Delta_r = -\frac{d\varphi_r}{dk_x}$. On the other hand, Fig. 5(d)-Fig. 5(f) illustrates the phase of the transmission coefficient (φ_t) as a function of the incidence angle for different values of defect mode wavelengths (λ_d). In contrast to the phase changes of the reflection coefficients, a remarkable negative slope appears near the incidence angles associated with the corresponding defect modes. Therefore, large positive values of positive GH shift are expected for the TM-polarized transmitted defect modes regarding the relation $\Delta_t = -\frac{d\varphi_t}{dk_x}$.

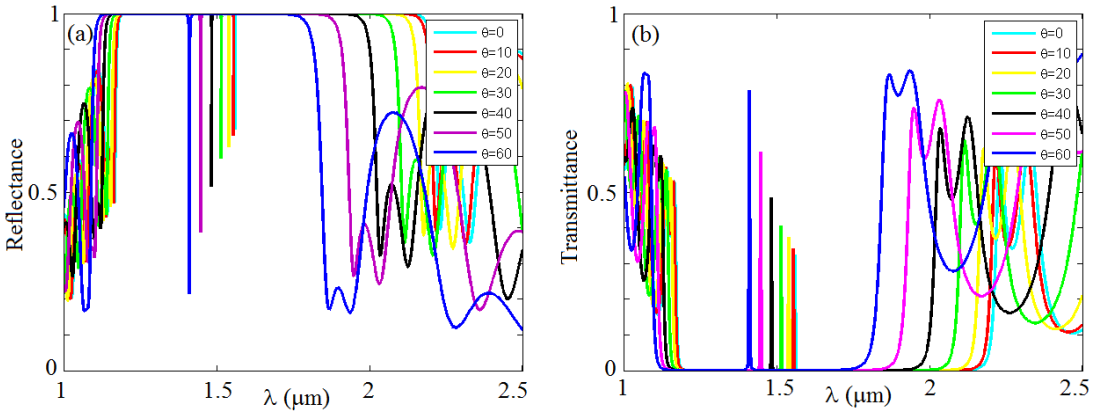


Fig. 4. (a) Reflection and (b) transmission spectra of the defective structure as a function of the wavelength for various incidence angles.

Table 1. The wavelength, reflectance, and transmittance of the defect modes and their corresponding incidence angles extracted from Fig. 4(a) and Fig. 4(b).

$\boldsymbol{\theta}$	$\mathbf{0}^{\circ}$	$\mathbf{10}^{\circ}$	$\mathbf{20}^{\circ}$	$\mathbf{30}^{\circ}$	$\mathbf{40}^{\circ}$	$\mathbf{50}^{\circ}$	$\mathbf{60}^{\circ}$
$\boldsymbol{\lambda_d}$	1559.6 nm	1554.3 nm	1538.8 nm	1514.2 nm	1482.5 nm	1446.5 nm	1409.9 nm
R	0.68	0.66	0.63	0.60	0.52	0.39	0.22
T	0.32	0.34	0.37	0.40	0.48	0.61	0.78

Fig. 6(a)-Fig. 6(f) illustrate the dependence of the GH lateral shifts of both reflected and transmitted beams on the incident angle, corresponding to the various defect-mode wavelengths summarized in Table 1. The lateral GH shifts were calculated using Eq. (5), assuming a beam width of $a = 50\lambda$. It is evident from Fig. 6(a)-Fig. 6(c) that the relative GH shifts of the reflected waves have negative values, which exhibit enhanced magnitudes around the incidence angles corresponding to the defect mode conditions. In contrast, Fig. 6(d)-Fig. 6(f) represent positive enhanced GH shifts of the transmitted defect modes. The magnitudes of the calculated relative GH shifts obtained from the plots of Fig.6 are listed in Table 2. As is evident from the data presented in Table 2, the magnitudes of the enhanced GH shifts of the reflected beams are in the range of $\Delta_r = -6.4\lambda$ to $\Delta_r = -9.5\lambda$, which are not significant values. Oppositely, the magnitudes of the enhanced GH shifts of the transmitted beams are in the range of $\Delta_t = +48.7\lambda$ to $\Delta_t = +89.7\lambda$ which are more noticeable compared to the values of Δ_r. So, it is expected that the detection and measurement of the GH shifts of the transmitted defect modes are feasible in the proposed defective structure.

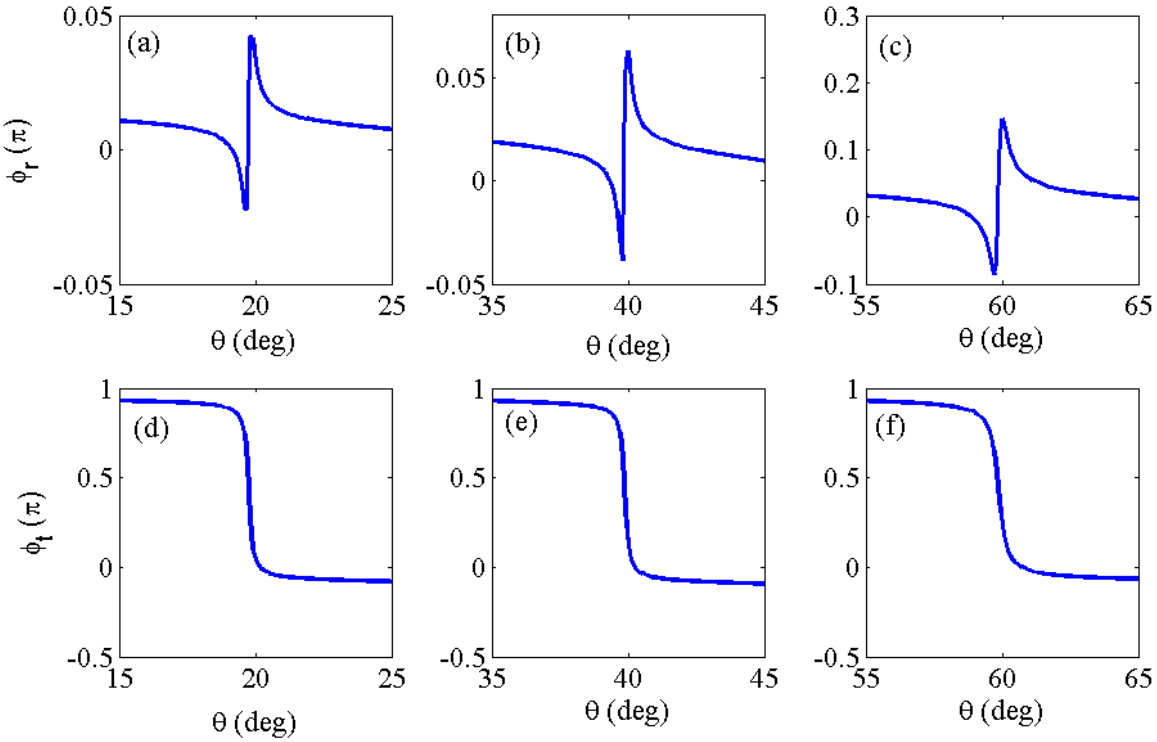


Fig. 5. The phase of the reflection coefficient (φ_r) as a function of the incidence angle for (a) $\lambda_d = 1538.8$ nm, $\theta = 20^\circ$, (b) $\lambda_d = 1482.5$ nm, $\theta = 40^\circ$ and (c) $\lambda_d = 1409.9$ nm, $\theta = 60^\circ$. The phase of the transmission coefficient (φ_t) as a function of the incidence angle for (d) $\lambda_d = 1538.8$ nm, $\theta = 20^\circ$, (e) $\lambda_d = 1482.5$ nm, $\theta = 40^\circ$ and (f) $\lambda_d = 1409.9$ nm, $\theta = 60^\circ$.

As a means of verifying the enhanced GH shift in the proposed design, the field distributions of the Gaussian beams, both before and after reflection and transmission, have been plotted in Fig. 7(a)-Fig. 7(c), for the case of $\lambda_d = 1409.9$ nm and $\theta = 60^\circ$ as functions of x. The negative displacement of the reflected beam and the positive displacement of the transmitted one have been shown clearly in part (b) and part (c) of Fig.7, respectively. It is evident from the figures that the magnitude of the GH shift for the transmitted beam is noticeably larger than that of the reflected beam.

Finally, we have investigated the effect of the filling factor (f) on the wavelength and the GH lateral shifts of the TM-polarized reflected and transmitted defect modes for the incidence angle of $\theta = 60^\circ$. Fig. 8(a)-Fig. 8(b) represent the reflection and transmission spectra of the defective structure for different values of the filling factor, respectively. It is evident from the figures that the wavelength of the defect mode shifts from $\lambda_d = 1409.9$ nm at $f = 0.8$ to $\lambda_d = 1296.9$ nm at $f = 0.4$. Also, the reflectance and the transmittance of the modes change slightly with changes in the filling factor. Fig.8(c)-Fig. 8(d) show the calculated GH shifts for the TM-polarized reflected and transmitted beams corresponding to the modes of Fig. 8(a)-Fig. 8(b). It is shown that the magnitudes of the GH shifts of the beams experience a slight decrease with a decrease in the filling fraction. So, we can say that the influence of the incidence angle on the GH shift of the beams is stronger than the effect of the filling factor.

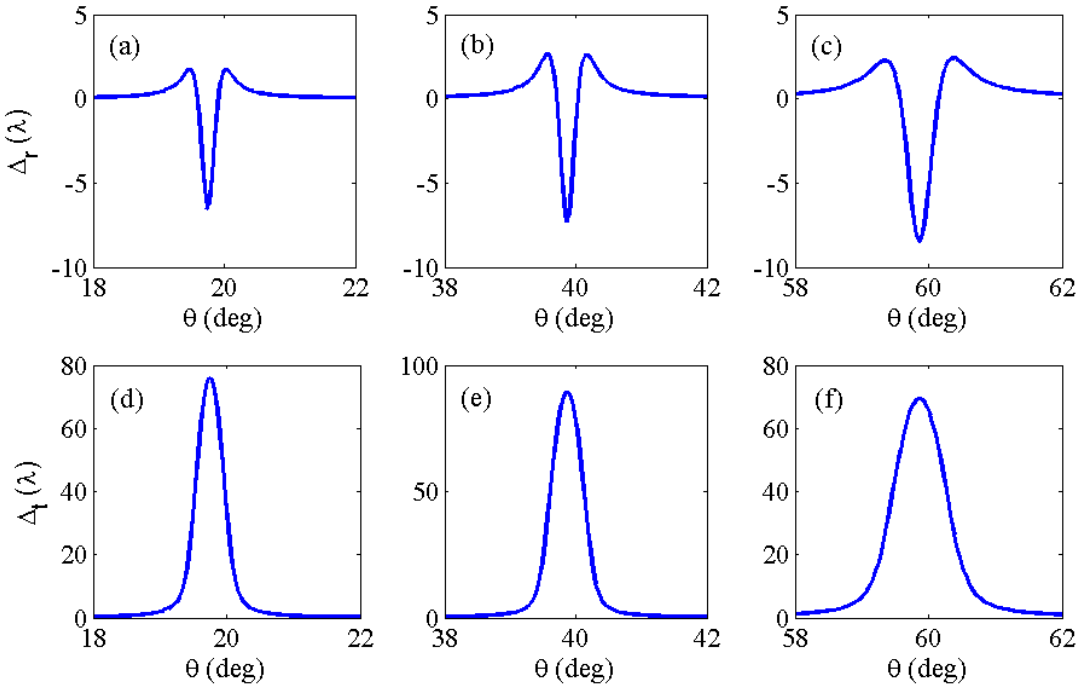


Fig. 6. The relative GH shifts of the reflected defect modes as a function of the incidence angle for the cases of (a) $\lambda_d = 1538.8$ nm, (b) $\lambda_d = 1482.5$ nm and (c) $\lambda_d = 1409.9$ nm. The relative GH shifts of the transmitted defect modes as a function of the incidence angle for the cases of (d) $\lambda_d = 1538.8$ nm, (e) $\lambda_d = 1482.5$ nm and (f) $\lambda_d = 1409.9$ nm.

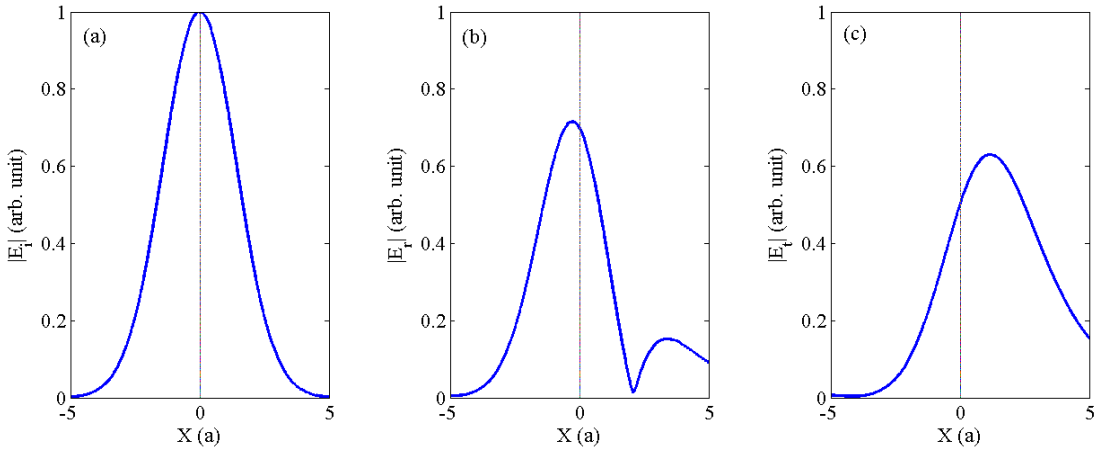


Fig. 7. The field profiles of (a) the incident, (b) the reflected, and (c) the transmitted Gaussian beams as functions of x for the case of $\lambda_d = 1409.9$ nm and $\theta = 60^{\circ}$.

4. Conclusion

This work is devoted to a theoretical study of the GH lateral shifts of TM-polarized reflected and transmitted defect modes within a defective one-dimensional photonic crystal. A layer of EMM has been considered as the defect layer of the proposed structure. The structure exhibited a wide PBG in the near-Infrared region with defect modes dependent on the angle of incidence. We have shown that increasing the incidence angle shifts the defect modes toward shorter wavelengths, where their reflectance and

transmittance vary noticeably. It was found that the increased GH shift can be experienced by the reflected and transmitted defect modes, where the sign of the shift is negative for the reflected modes and positive for the transmitted ones. The results showed that the maximum value of $\Delta_r = -9.5\lambda$ at $\lambda_d = 1409.9$ nm and $\theta = 60^\circ$, and $\Delta_t = +89.7\lambda$ at $\lambda_d = 1482.5$ nm and $\theta = 40^\circ$ can be obtained for the reflected and transmitted modes, respectively. This enhanced GH shift around the reflected and transmitted defect modes has been verified by plotting the field distribution of the incident, reflected, and transmitted waves for the case of $\lambda_{TPP} = 1409.9$ nm and $\theta = 60^\circ$. Also, the effect of the filling factor on the wavelength and GH shift of the defect modes has been investigated. It is found that the change in the filling factor shifts the wavelengths of the defect modes; however, it has no noticeable effect on the magnitudes of the GH shifts.

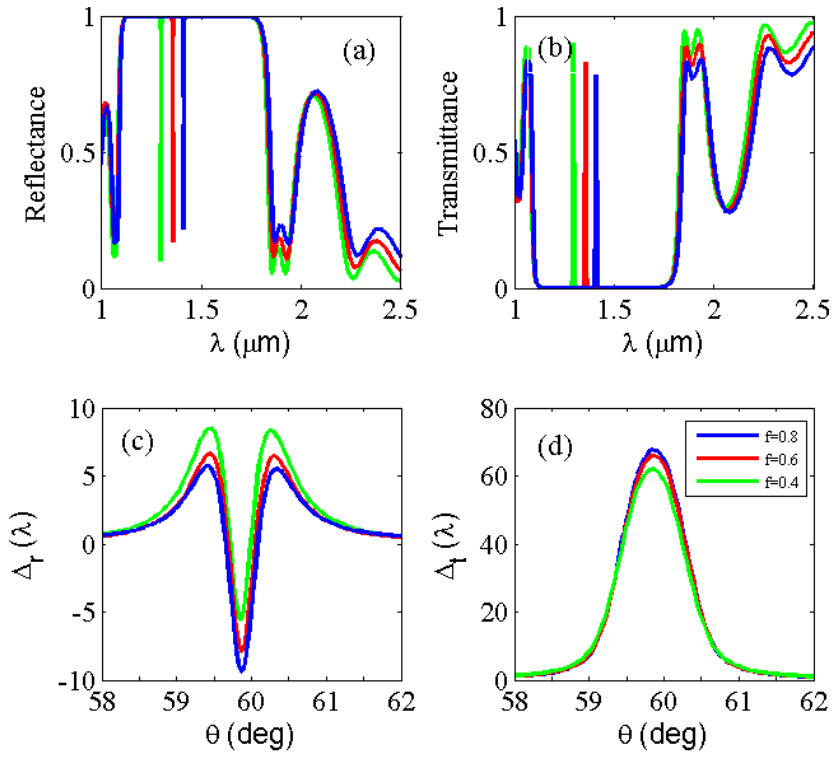


Fig. 8. (a) Reflection and (b) transmission spectra of the defective structure as a function of the wavelength for various filling factors. (c) The GH shift of the reflected and (d) the transmitted defect modes as a function of the incidence angle for various filling factors.

5. Declarations Conflict of Interest

The authors declare that they have no known competing financial interests or personal relationships that could have appeared to influence the work reported in this paper.

References

[1] F. Goos, H. Hänchen, Ein neuer und fundamentaler Versuch zur Totalreflexion, Annalen der Physik, 436 (1947) 333-346.
[2] K. Artmann, Berechnung der Seitenversetzung des totalreflektierten Strahles, Annalen der Physik, 437 (1948) 87-102.

[3] P. Balcou, L. Dutriaux, Dual optical tunneling times in frustrated total internal reflection, Physical review letters, 78 (1997) 851.
[4] M.A. Porras, Nonspecular reflection of general light beams at a dielectric interface, Optics communications, 135 (1997) 369-377.
[5] A. Haibel, G. Nimtz, A. Stahlhofen, Frustrated total reflection: The double-prism revisited, Physical Review E, 63 (2001) 047601.
[6] T. Tang, C. Li, L. Luo, Y. Zhang, J. Li, Goos–Hänchen effect in semiconductor metamaterial waveguide and its application as a biosensor, Applied Physics B, 122 (2016) 167.
[7] X. Wang, C. Yin, J. Sun, H. Li, Y. Wang, M. Ran, Z. Cao, High-sensitivity temperature sensor using the ultrahigh order mode-enhanced Goos-Hänchen effect, Optics Express, 21 (2013) 13380-13385.
[8] K.V. Sreekanth, Q. Ouyang, S. Sreejith, S. Zeng, W. Lishu, E. Ilker, W. Dong, M. ElKabbash, Y. Ting, C.T. Lim, Phase-change-material-based low-loss visible-frequency hyperbolic metamaterials for ultrasensitive label-free biosensing, Advanced Optical Materials, 7 (2019) 1900081.
[9] T. Shui, W.-X. Yang, Q. Zhang, X. Liu, L. Li, Squeezing-induced giant Goos-Hänchen shift and hypersensitized displacement sensor in a two-level atomic system, Physical Review A, 99 (2019) 013806.
[10] H.-E. Horng, C. Chen, K. Fang, S. Yang, J. Chieh, C.-Y. Hong, H. Yang, Tunable optical switch using magnetic fluids, Applied physics letters, 85 (2004) 5592-5594.
[11] Y. Nie, Y. Li, Z. Wu, X. Wang, W. Yuan, M. Sang, Detection of chemical vapor with high sensitivity by using the symmetrical metal-cladding waveguide-enhanced Goos-Hänchen shift, Optics Express, 22 (2014) 8943-8948.
[12] Y.V. Bludov, M.I. Vasilevskiy, N.M.R. Peres, Tunable graphene-based polarizer, Journal of Applied Physics, 112 (2012).
[13] F. Bretenaker, A. Le Floch, L. Dutriaux, Direct measurement of the optical Goos-Hänchen effect in lasers, Physical review letters, 68 (1992) 931.
[14] Y. Wang, Y. Liu, B. Wang, Tunable electron wave filter and Goos–Hänchen shift in asymmetric graphene double magnetic barrier structures, Superlattices and Microstructures, 60 (2013) 240-247.
[15] C. Luo, J. Guo, Q. Wang, Y. Xiang, S. Wen, Electrically controlled Goos-Hänchen shift of a light beam reflected from the metal-insulator-semiconductor structure, Optics express, 21 (2013) 10430-10439.
[16] C.G. Avendaño, I. Molina, J.A. Reyes, Anchoring effects on the electrically controlled optical band gap in twisted photonic liquid crystals, Liquid Crystals, 40 (2013) 172-184.
[17] J.-S. Li, J.-f. Wu, L. Zhang, Tunable terahertz wave Goos–Hänchen shift of reflected terahertz wave from prism–metal–polymer–metal multilayer structure, Optics Communications, 334 (2015) 101-104.
[18] P. Ma, L. Gao, Large and tunable lateral shifts in one-dimensional PT-symmetric layered structures, Optics Express, 25 (2017) 9676-9688.
[19] D. Zhao, W.-w. Liu, S.-l. Ke, Q.-j. Liu, Large lateral shift in complex dielectric multilayers with nearly parity–time symmetry: D. Zhao et al, Optical and Quantum Electronics, 50 (2018) 323.
[20] V. Moskalenko, I.V. Soboleva, A.A.e. Fedyanin, Surface wave-induced enhancement of the Goos-Hänchen effect in one-dimensional photonic crystals, Jetp Letters, 91 (2010) 382-386.
[21] I. Soboleva, V. Moskalenko, A. Fedyanin, Giant Goos-Hänchen effect and Fano resonance at photonic crystal surfaces, Physical review letters, 108 (2012) 123901.
[22] Y.S. Dadoenkova, N. Dadoenkova, I. Lyubchanskii, Y. Lee, T. Rasing, Effect of lateral shift of the light transmitted through a one-dimensional superconducting photonic crystal, Photonics and Nanostructures-Fundamentals and Applications, 11 (2013) 345-352.

[23] Z. Xiao, H. Luo, S. Wen, Goos-Hänchen and Imbert-Fedorov shifts of vortex beams at air–left-handed-material interfaces, Physical Review A—Atomic, Molecular, and Optical Physics, 85 (2012) 053822.
[24] D.-K. Qing, G. Chen, Goos–Hänchen shifts at the interfaces between left-and right-handed media, Optics Letters, 29 (2004) 872-874.
[25] X. Chen, C.-F. Li, Lateral shift of the transmitted light beam through a left-handed slab, Physical Review E—Statistical, Nonlinear, and Soft Matter Physics, 69 (2004) 066617.
[26] F. Lima, T. Dumelow, E. Albuquerque, J. Da Costa, Power flow associated with the Goos-Hänchen shift of a normally incident electromagnetic beam reflected off an antiferromagnet, Physical Review B—Condensed Matter and Materials Physics, 79 (2009) 155124.
[27] P. Gruszecki, M. Mailyan, O. Gorobets, M. Krawczyk, Goos-Hänchen shift of a spin-wave beam transmitted through anisotropic interface between two ferromagnets, Physical Review B, 95 (2017) 014421.
[28] Q. Cheng, T.J. Cui, Lateral shifts of optical beams on the interface of anisotropic metamaterial, Journal of applied physics, 99 (2006).
[29] M. Cheng, R. Chen, S. Feng, Lateral shifts of an optical beam in an anisotropic metamaterial slab, The European Physical Journal D, 50 (2008) 81-85.
[30] H. Lai, S. Chan, W. Wong, Nonspecular effects on reflection from absorbing media at and around Brewster's dip, Journal of the Optical Society of America A, 23 (2006) 3208-3216.
[31] B. Zhao, L. Gao, Temperature-dependent Goos-Hänchen shift on the interface of metal/dielectric composites, Optics express, 17 (2009) 21433-21441.
[32] L.-G. Wang, H. Chen, S.-Y. Zhu, Large negative Goos–Hänchen shift from a weakly absorbing dielectric slab, Optics letters, 30 (2005) 2936-2938.
[33] D. Jahani, O. Akhavan, A. Hayat, M. Shah, Optical Goos–Hänchen effect in uniaxially strained graphene, Journal of the Optical Society of America A, 40 (2022) 21-26.
[34] S. Chen, C. Mi, L. Cai, M. Liu, H. Luo, S. Wen, Observation of the Goos-Hänchen shift in graphene via weak measurements, Applied Physics Letters, 110 (2017).
[35] S. Shirin, A. Madani, S.R. Entezar, Tunable lateral shift of the reflected optical beams from a nanocomposite structurally chiral medium, Optical Materials, 107 (2020) 110026.
[36] S. Shirin, A. Madani, S.R. Entezar, Electrically controlled lateral shift of the reflected optical beams from a nanocomposite structurally chiral medium, Physica Scripta, 95 (2020) 095504.
[37] S. Shirin, A. Madani, S.R. Entezar, Polarization switchable lateral shift of the transmitted and reflected defect modes from a structurally chiral medium with a twist defect, Physica Scripta, 100 (2025) 085567.
[38] P. Xiao, Beam reshaping in the occurrence of the Goos–Hänchen shift, Journal of the Optical Society of America B, 28 (2011) 1895-1898.
[39] M. Jezzini, J. Gutierrez-Vega, The Goos-Hanchen shift in Helmholtz-Gauss beams, SPIE2006.
[40] X. Yang, T. Qu, Z. Li, Z. Wu, Spatial Goos–Hänchen Shifts of Airy Vortex Beams Impinging on Graphene/hBN Heterostructure, Photonics, MDPI, 2025, pp. 105.
[41] W. Zhen, D. Deng, Goos-Hänchen shifts for Airy beams impinging on graphene-substrate surfaces, Optics Express, 28 (2020) 24104-24114.
[42] L. Lambrechts, V. Ginis, J. Danckaert, P. Tassin, Transformation optics approach for Goos-Hänchen shift enhancement at metamaterial interfaces, Metamaterials X, SPIE, 2016, pp. 149-155.
[43] N. Goswami, A. Kar, A. Saha, Long range surface plasmon resonance enhanced electro-optically tunable Goos–Hänchen shift and Imbert–Fedorov shift in ZnSe prism, Optics Communications, 330 (2014) 169-174.
[44] N. Shaabani, A. Madani, M. Shiri, R. Abdi-Ghaleh, Goos–Hänchen effect on a graphene-based hyperbolic metamaterial slab: N. Shaabani et al, Applied Physics A, 126 (2020) 775.

[45] L. Chen, X. Liu, Z. Cao, S. Zhuang, Mechanism of giant Goos–Hänchen effect enhanced by long-range surface plasmon excitation, Journal of optics, 13 (2011) 035002.
[46] A. Madani, S.R. Entezar, Tunable enhanced Goos–Hänchen shift in one-dimensional photonic crystals containing graphene monolayers, Superlattices and Microstructures, 86 (2015) 105-110.
[47] L.-G. Wang, S.-Y. Zhu, Giant lateral shift of a light beam at the defect mode in one-dimensional photonic crystals, Optics letters, 31 (2006) 101-103.
[48] Y. Chen, P. Hou, M. Shen, J. Shi, Q. Wang, Goos-Hiichen shifts for a one-dimensional photonic crystal with a nonlinear defect, 2006 International Symposium on Biophotonics, Nanophotonics and Metamaterials, IEEE, 2006, pp. 328-331.
[49] D. Zhao, F. Liu, P. Meng, J. Wen, S. Xu, Z. Li, D. Zhong, Reflection enhancement and giant lateral shift in defective photonic crystals with graphene, Applied Sciences, 9 (2019) 2141.
[50] X. Yang, Z. Liao, Z. Chu, X. Zhu, H. Da, Enhanced Goos–Hänchen shift in a defective Pell quasiperiodic photonic crystal with monolayer MoS2, Applied Optics, 62 (2023) 5861-5866.
[51] A. Ashenaei, K. Jamshidi-Ghaleh, R. Abdi-Ghaleh, Goos–Hänchen shift in a 1D-photonic crystal structure containing a Weyl semimetal defect layer, Applied Optics, 64 (2025) 6432-6438.
[52] A.A. Sayem, M. Mahdy, M.S. Rahman, Broad angle negative refraction in lossless all dielectric or semiconductor based asymmetric anisotropic metamaterial, Journal of Optics, 18 (2016) 015101.
[53] Y. She, J. Ruan, D. Liu, M. Yao, C. Yin, K. Xu, F. Wu, Tunable high-performance polarization selectivity empowered by polarization-sensitive Fabry-Perot modes in one-dimensional photonic crystals containing an elliptical metamaterial defect, Physica Scripta, 100 (2025) 055505.
[54] S. Jahani, Z. Jacob, Transparent subdiffraction optics: nanoscale light confinement without metal, Optica, 1 (2014) 96-100.
[55] F. Wu, S. Xiao, Tamm plasmon polariton with high angular tolerance in heterostructure containing all-dielectric elliptical metamaterials, Physica B: Condensed Matter, 649 (2023) 414502.
[56] Z. Cheng, Y. She, A. Panda, M. Feng, J. Li, F. Wu, Ultra-large near-infrared omnidirectional photonic bandgaps in cascaded one-dimensional photonic crystals containing all-dielectric metamaterials, Applied Optics, 62 (2023) 6625-6630.
[57] F. Wu, T. Liu, M. Chen, S. Xiao, Photonic bandgap engineering in hybrid one-dimensional photonic crystals containing all-dielectric elliptical metamaterials, Optics Express, 30 (2022) 33911-33925.
[58] A. Borghesi, G. Guizzetti, E. Palik, Handbook of Optical Constants of Solids, New York: Academic, DOI (1985) 445-464.
[59] L. Brekhovskikh, R. Beyer, Elsevier Science Technology (Firm). Waves in Layered Media, Applied mathematics and mechanics. Academic Press, DOI (1980).
[60] S. De Leo, G.G. Maia, Lateral shifts and angular deviations of Gaussian optical beams reflected by and transmitted through dielectric blocks: a tutorial review, Journal of Modern Optics, 66 (2019) 2142-2194.
[61] A. Madani, S.R. Entezar, Optical properties of one-dimensional photonic crystals containing graphene-based hyperbolic metamaterials, Photonics and Nanostructures-Fundamentals and Applications, 25 (2017) 58-64.